Journal of Chromatography, 149 (1978) 29–42

CHROM. 10,833

COMPARISON OF BROADENING PATTERNS IN REGULAR AND RADIALLY COMPRESSED LARGE-DIAMETER COLUMNS

CLAUDE H. EON

Département de Chimie, Université de Sherbrooke, Sherbrooke, Québec J1K 2R1 (Canada)

SUMMARY

The differential broadening pattern of an inert solute injected centrally into a regular (A) and a radially compressed (B) column has been studied. The two columns exhibit identical properties when operated in the infinite diameter mode.

A marked difference, to the advantage of column B, develops as the solute becomes appreciably exposed to the wall region. At its fullest extent, the wall effect accounts for a nearly 2.5-fold increase in plate height for column A compared with a 1.5-fold increase for column B.

This behaviour is rationalized in terms of a semi-theoretical model that takes the radial diffusivity, the radial dependence of the lateral plate height and the peak local velocity into account. It is further shown that the solute radial concentration profile departs significantly from a truncated gaussian shape. The actual profile can be expressed as a Bessel function series.

INTRODUCTION

Despite the great amount of attention devoted to column performance, the extent of the wall effect is still poorly understood. This effect causes packing heterogeneities and distorts the flow profile, causing the overall axial dispersion to increase. In comparison with short-range effects (diffusion, anastomosis etc.), wall-induced long-range contributions are less amenable to adequate modelling, as this would involve functional relationships between actual diffusivities and velocity with radial position.

As the nature of these relationships is unknown, an analytical solution of the problem is not yet possible. Hence we are still in urgent need of accurate experimental data to refine and promote new theories, and the study described here originated from this need. This is by no means a new concern if we recall the early contributions by Huyten *et al.*[1], Sie and Rijnders[2], Frisone[3], Giddings[4], Giddings and Fuller[5], Littlewood[6,7], Hupe *et al.*[8], Golay[9] and others[10,11], which have been reviewed by Conder[12]. However, these studies revealed some contradictions and are difficult to transpose to liquid chromatography.

In this mode of chromatography, the work of Knox is most important. Of his various studies[13–16], two are of special interest in the present context. In the first,

Knox and Parcher[15] formulated a set of operating conditions for minimizing the wall effect by confining most of the solute into the central core of the column; they also showed how the plate height could be calculated from Giddings' non-equilibrium theory[17] if the velocity profiles were known. In the second, Knox *et al.*[16] refined their previous findings and introduced the use of a dual polarographic detector for the precise determination of radial dispersion. Other pertinent details regarding the wall effect and radial mixing can be found elsewhere[18,19]. In this paper, we consider the still puzzling facets of the problem: the extent of the wall effect, the angular symmetry of the packing network and the way and the extent to which the efficiency gradually deteriorates as the solute moves nearer the wall. Also, the potential benefit of using the newly introduced radially compressed columns[20] has been investigated in terms of a less detrimental wall effect. Because of its unmatched capabilities, the dual polarographic detector was used here, so that this study is similar to and complements the work of Knox *et al.*[16].

EXPERIMENTAL

It was considered that the study of an inert probe eluted through a glass bead column would reveal the most striking features of the wall effect. In addition to allowing a comparison with existing data[14], such a system facilitates any subsequent theoretical interpretation in that it is free from chromatographic secondary effects (mass transfer involving the stagnant mobile phase, etc.), which, by their action on the overall result, might hide some intrinsic properties of the main flow.

Two 60 × 2.2 cm O.D. columns were considered. The first, an internally polished stainless-steel column, had an I.D. of 1.73 cm and the second, made of Teflon, had an I.D. of 1.58 cm. By adopting common standard conditions, the two columns can be compared regardless of the small difference in inner diameter. Both columns were dry packed with glass beads according to the procedure described by Snyder and Kirkland[21]. Microscopic measurements showed that the beads has a mean diameter of 76 μm with a standard deviation of 6 μm. Note that the ratio of the column to the particle diameter is typical of those encountered in analytical systems.

After filling and testing the two columns several times, we were able to obtain two quasi-identical core packing properties; this was a prime requirement for this study. Of course, the Teflon column had to be radially compressed prior to any testing; this was done by jacketing the column over 57 cm of its length and by pressurizing the system with nitrogen. The radial pressure was usually kept at least 50 bar higher than the column operating pressure. The various other fittings and the dual polarographic detector designs were taken from Knox *et al.*[16] and need not be described here. The only major difference is that the detection block was made to withstand pressures of 100–150 bar by replacing all O-rings (except that related to the movable electrode) by Swagelok fittings. For the movable electrode, a hollow screw was used to compress the O-ring so as to ensure adequate water tightness. The platinum electrodes consisted of two spherical electrodes of diameter 0.2 mm; they were held 0.1 mm below the external surface of the outlet frit. The procedure for measuring the radial concentration profiles was also described by Knox *et al.*[16].

The tracer was injected centrally into the top of the column by means of a syringe; the needle, which slid in a central guide, was allowed to penetrate 1 cm into

the packing. The volumes injected varied from 1 to 5 μl so that an adequate solute concentration within the detector chamber was ensured. The movable electrodes monitored the solute concentration in comparision with that of a reference point, usually the centre of the column. The two currents were simultaneously recorded, thus permitting the peak radial concentration and relative velocity and the radial dependence of the longitudinal plate height to be obtained. Successive experiments, with the movable electrode located at different positions, gave all of the necessary data. The supporting electrolyte was 0.1 *M* potassium chloride solution kept free from oxygen; the probe was *p*-nitrophenol.

A special arrangement was used in order to investigate the deterioration of the column performance as the solute became more exposed to the wall. Only two operating changes favour radial dispersion, each of which is inconvenient in practice: either the flow velocity is reduced or the column is lengthened.

The first alternative should be avoided because it also changes the extent of the axial dispersion; the second should also be rejected as it involves re-packing the column, which may lead to significantly different bed structures. Instead, we chose to increase the distance travelled by the solute artificially without increasing the column length. It suffices to reverse the direction of flow alternately, so that the solute travels back and forth within the column until it is allowed to leave. Adequate timing permits the path travelled to be lengthened at will; the volume of eluent collected from the injection time is measured. The arrangement is outlined in Fig. 1.

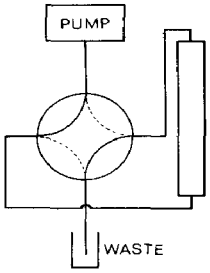

Fig. 1. Schematic diagram of the system.

This method has certain drawbacks. As the flow profile is not flat, reversing the direction of flow must distort the solute profile. It is conceivable, however, that, after a while, the faster moving zones regain their position with respect to the average peak velocity so that the zone overall second moment is not greatly affected; this, however, has not been proved. However, no significant changes were found, provided that the amplitude of the back and forth movement was sufficiently large. Hence care was taken to reverse the flow as seldom as possible; furthermore, the last trajectory was always greater than 25–30 cm.

RESULTS AND DISCUSSION

Columns operated in the infinite diameter mode

Although the ultimate aim of this study was to compare the two types of columns in terms of their overall axial plate heights, it is first illustrative to consider

their respective "core" axial and radial plate heights. The first property is easily obtained by monitoring the solute concentration at the centre of the column outlet. The latter was calculated from the radial concentration profile by assuming that the columns were operated in the infinite diameter mode. This assumption will be justified latter; for now it is sufficient to say that it held fairly true for $\nu \geqslant 15$ (ν = reduced velocity).

Prior to describing the results, it may be worthwhile reviewing some of the basic differences between radial and longitudinal dispersion. The radial plate height (H_r) and the axial plate height (H_a) can be defined as the increase in variance measured in the radial (σ_r^2) and axial (σ_a^2) directions, respectively, per unit column length:

$$H_r \equiv \frac{\mathrm{d}\sigma_r^2}{\mathrm{d}l} \qquad H_a \equiv \frac{\mathrm{d}\sigma_a^2}{\mathrm{d}l} \tag{1}$$

Dividing the two quantities by the mean particle diameter (d_p) leads to the corresponding reduced plate heights, h_r and h_a, which will be used here. Assuming that the broadening occurs as the results of a diffusion-like process, the plate heights are related to the apparent or overall diffusivities, D_r and D_a, through the classical relationships[14,17]

$$H_r \equiv \frac{2\,D_r}{u} \qquad H_a \equiv \frac{2\,D_a}{u} \tag{2}$$

where u is the linear velocity of the carrier. Note that the diffusivity under carrier movement is anisotropic in nature so that D_r and D_a always differ, even for an ideal isotropic column. For glass bead columns, the relationship between the reduced plate height and the carrier velocity takes the simplest form as virtually no mass transfer occurs between the mobile and stationary phases.

Hence the simplest equations are expected to describe the experimental results[14,22]:

$$h_r = \frac{B}{\nu} + C \qquad h_a = \frac{B}{\nu} + A\nu^d \tag{3}$$

where ν (the reduced velocity) is defined as $\nu = ud_p/D_m$, where D_m is the probe molecular diffusion coefficient within the carrier. It is easily recognized that the B/ν term, which is common to both equations, accounts for the molecular diffusion. As the latter is somehow impeded by the packing, B is always less than 2, as implied by eqn. 2.

The C term arises from "stream splitting", the mechanism of which has been described in the chemical engineering literature[23,24] and by Littlewood[7] and Horne *et al.*[14] from the chromatographic point of view. Typical values of C range between 0.05 and 0.2. On the other hand, the $A\nu^d$ term accounts for the coupling effect[17]. Typical values of A and d are 0.5–1 and 0.25–0.35, respectively.

In spite of their semi-empirical nature, eqns. 3 have proved useful for fitting purposes within the laminar velocity range.

Both radial and central axial plate heights for the two columns under study are given in Fig. 2. It should be noted that the two columns are expected to exhibit the

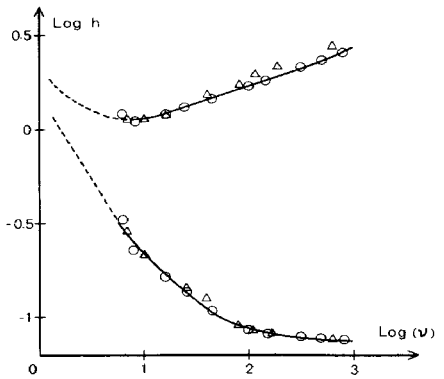

Fig. 2. Reduced central axial plate height (upper curve) and radial plate height (lower curve). ○, Classical column; △, radially compressed column.

same core properties so that any subsequent difference can be attributed only to the wall effect. The coefficients used for the calculation of the solid lines are $A = 0.64$, $B = 1.5$, $C = 0.075$ and $d = 0.21$.

The results compare fairly well with those described by Knox *et al.*[16], but the axial plate height is slightly better and the radial plate height is slightly worse here, as Knox *et al.*[16] reported a value of 0.06 for the C term. Nevertheless, the greatest interest of Fig. 2 is that it illustrates the similarity of the bulk columns. As pointed out before, the two columns were assumed to be operated in the infinite diameter mode; this is a good approximation for $\nu > 15$. The next section is concerned with the gradual departure from this idealized situation.

Radial dispersion in relation to the wall effect

Under the assumption of infinite diameter operation, no significant amount of solute reaches the wall, but we should consider what happens when this is not so. As radial diffusion is obstructed by the wall, a build-up of solute concentration is likely to develop in the vicinity of the wall. The new concentration profile, which departs from its limiting gaussian shape, could be calculated from the mass balance equation for the system.

Assuming an angular symmetry and assuming that D_r, D_a and u are functions $D_r(r)$, $D_a(r)$ and $u(r)$ of the radial position r, then

$$\frac{\partial C}{\partial t} = -u(r) \cdot \frac{\partial C}{\partial l} + \frac{\partial}{\partial l} \cdot D_a(r) \cdot \frac{\partial C}{\partial l} + \frac{1}{r} \cdot \frac{\partial}{\partial r} \cdot r\, D_r(r) \cdot \frac{\partial C}{\partial r} \qquad (4)$$

where C is the solute concentration. Unless the exact natures of $D_r(r)$, $D_a(r)$ and $u(r)$ are known, eqn. 4 cannot be solved. Note that this lack of an adequate model illustrates the need for studies such as that described here. Nevertheless, it is useful to consider the solution of eqn. 4 under the assumption of an isotropic medium. Any departure from this theoretical profile can subsequently be attributed to the wall effect. The main boundary condition is

$$\frac{\partial C}{\partial r} = 0 \qquad \text{at} \qquad r = R \qquad (5)$$

where R is the radius of the column. Eqns. 4 and 5 have been solved by Klinkenberg *et al.*[25]; the radial concentration profile taken at the retention time when half of the peak has left the column is

$$C(r) = C_0\left\{1 + \tfrac{1}{2}\sum_{a_1 > 0}^{\infty} \frac{1}{Q}\exp\left[\left(\tfrac{1}{2} - Q\right)\frac{uRL}{D_a}\right] \cdot \frac{J_0(a_1\,\bar{r})}{J_0^2(a_1)}\right\} \tag{6}$$

where C_0 is the initial tracer concentration and

$$Q = \left(\tfrac{1}{4} + \frac{(a_1 uR)^2}{D_a D_r}\right)^{\frac{1}{2}}$$

The reduced diameter, $\bar{r}$, is defined as r/R. J_0 is the zeroth Bessel function and a_1 are the roots of the equation $J_1(a_1) = 0$. Eqn. 6 converges rapidly so that the first few a_1 values need to be considered. It is interesting to compare how eqn. 6 gradually departs from a purely gaussian curve. As it depends upon the system parameters, it is convenient to express the column length by reference to an arbitrary length, L_1, defined in such a way that it normalizes the system with respect to the radial concentration function. Let L_1 be the length for which the peak variance is one quarter of the column radius. As the solute concentration at the wall is very small, the use of the gaussian model is justified. Hence, by combining eqns. 1 and 3 we obtain

$$L_1 = \frac{R^2}{d_p}\,\frac{1}{16[(B/\nu) + C]} \tag{7}$$

Then the ratio L/L_1 for any system fully characterizes the extent of the radial dispersion.

Fig. 3 shows the concentration profiles calculated from eqn. 6 for several L/L_1 ratios. Note that the concentration is expressed on a relative basis as $C = C(\bar{r})/C_0$. It is observed that eqn. 6 differs appreciably from the perfect gaussian shape, particularly for long columns; eventually the radial concentration becomes uniform. This was not a problem in the work of Knox *et al.*[16], as their actual concentration profiles departed only slightly from the gaussian distribution. Fig. 3, if validated, enables one to visualize the extent of the gradual exposure of the solute to the wall effect, which is of paramount importance in liquid chromatography. As it was derived with the assumption of an isotropic column, it is essential to investigate its ability to account for real column behaviour. This was done by artificially increasing the column length, as described previously. Surprisingly, most of our preliminary results validate the use of eqn. 6, even though the classical column exhibits a strong wall effect. As a typical example, Fig. 4 shows the results obtained with the stainless-steel column operated at $\nu = 100$. It is noticeable. that no significant deviation from the theoretical curve occurs in the vicinity of the wall. A possible explanation is that two opposing effects roughly cancel out. The relatively low density in the region of the wall promotes an increase in both axial and radial diffusivities; the former tends to flatten the concentration profile while the latter favours a local enrichment through

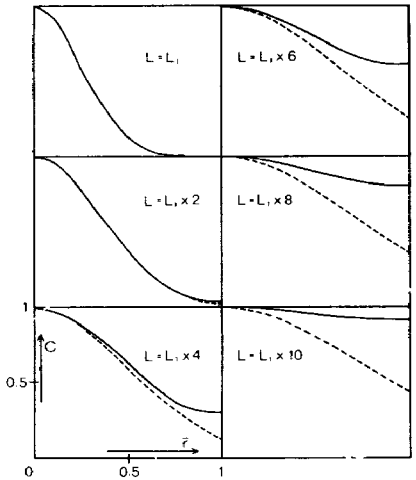

Fig. 3. Comparison of the radial concentration profiles, expressed on a relative basis, as a function of the reduced column length and reduced radius. Solid lines, calculated from eqn. 6; broken lines, calculated assuming a truncated gaussian function (eqn. 12 from ref. 15).

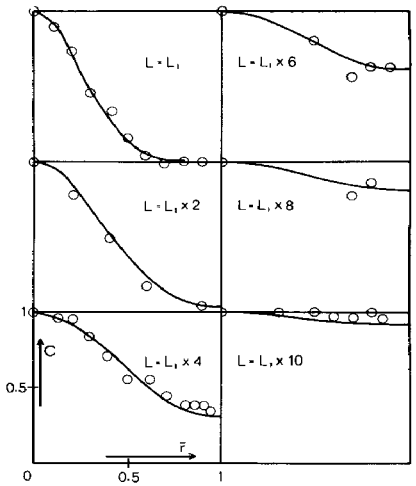

Fig. 4. Peak height *versus* radial position for the stainless-steel column operated at $\nu = 100$. $L_1 = 68.5$ cm. The solid lines give the best fit in term of eqn. 6.

trans-column mass transfer. Hence, until further data are available, it can be assumed that the apparent radial diffusivity is not greatly affected by the disorder in the wall region. Results for the Teflon column are very similar to those in Fig. 4. As mentioned before, the graph of radial plate height *versus* velocity in Fig. 2 was obtained by assuming that the two columns were operated in a quasi-infinite diameter mode. This approximation was found to be reasonable for $\nu > 15$, a range of velocity for which the reduced column length (L/L_1) was always less than 2. Fig. 2 and 3 confirm that no significant deviation from the gaussian curve occurred. The two radial plate heights measured for $\nu < 15$ were calculated on the basis of eqn. 6.

Radial dependence of the longitudinal plate height and column angular symmetry

The results were obtained according to the method described by Knox *et al.*[16], except that eight concentric directions were investigated and averaged in order to offset the angular column asymmetry. The results are now related to the actual column length (60 cm) as the direction of flow was unchanged during the experiments. Two properties are of interest: the axial plate height *versus* radial position and its corresponding peak velocity compared with the average carrier velocity. Because of the heterogeneity of the packing, the tracer transit time is expected to vary with the radial position. By monitoring the output at different points of the column exit it is therefore possible to calculate the apparent integrated peak velocity relative to the carrier velocity ($u/\bar{u}$). Results for the two columns operated at $\nu = 100$ are reported in Figs. 5 and 6. Comparison of the two sets of results reveals some analogies and differences.

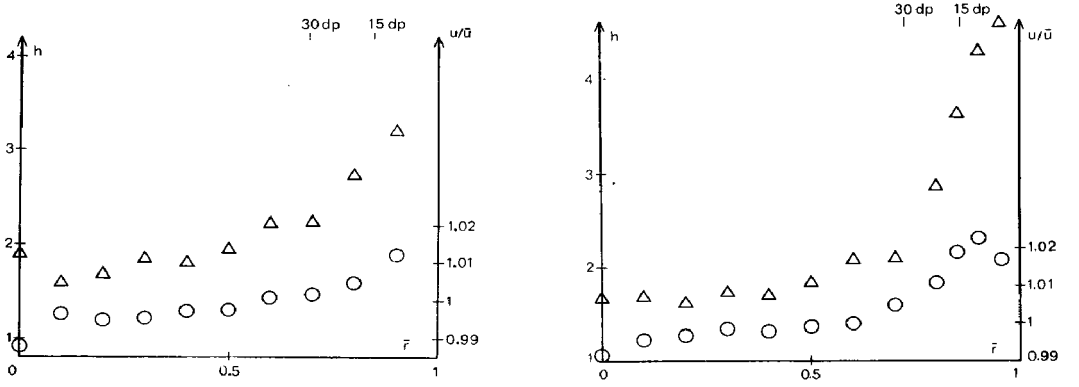

Fig. 5. Dependence of the axial reduced plate height (△) and peak maximum relative velocity (○) on the reduced radial position for the classical column operated at $\nu = 100$.

Fig. 6. As Fig. 5, but for the Teflon column.

In both instances, the reduced plate height gradually increases from the centre of the column to the wall. A transition occurs at 20–30 particle diameters from the wall, in agreement with the finding of Knox *et al.*[16], and confirms that the wall effect extends further than was first thought[15]. However, as the wall effect gradually smooths out, any geometric definition of the disturbed zone is arbitrary. Although the two columns exhibit similar core properties, the stainless-steel column (A) is more disturbed than the Teflon column (B) by the wall. For $\bar{r} = 0.9$, column A exhibits a reduced plate height 30% larger than that of column B. In addition, there is a strong correlation between the reduced plate height and the apparent velocity of the solute. As pointed out by Knox *et al.*[16], it is important to bear in mind that the apparent velocity of the peak maximum is not the same as the velocity of the eluent at any distance along the axis because of radial mixing. For the same reason, $(u/\bar{u})_r$ is not constant throughout the column; it is an integrated quantity from the column inlet to the point of measurement. However, the $(u/\bar{u})_r$ function must be related somehow to both the local eluent velocity and column porosity. It is tempting to identify the increases in both h and $u/\bar{u}$ in the vicinity of the wall as a reflection of the degradation of the packing tightness.

In a similar manner, the column axis appears to be the densest part of the network. Assuming that the overall tracer zone moves at the average velocity of the carrier, then $(u/\bar{u})_{r=1}$ can be estimated for

$$2\int_0^1 \bar{r}(u/\bar{u})\, d\bar{r} \equiv 1$$

Use of the trapeze rule leads to $(u/\bar{u})_{r=1} \approx 0.9985$ for both columns. The decrease in $u/\bar{u}$ arises from two opposing effects: the deterioration of the packing density, which would contribute to an increase in $u/\bar{u}$, and the zero velocity at the carrier–wall interface, which offsets the former.

As pointed out before, the results in Figs. 5 and 6 were obtained by averaging the properties of eight concentric directions. Such experiments provide valuable information on the angular symmetry of the packing network. As a rule, the Teflon column exhibits better angular symmetry than column A.

Typical results for the more disturbed regions of column A are illustrated in Fig. 7. The strong correlation between $u/\bar{u}$ and h is still observed but the most striking feature is that this plot shows the existence of long-range packing disorders. For example, the packing density in direction A is constantly better than in directions D–E,

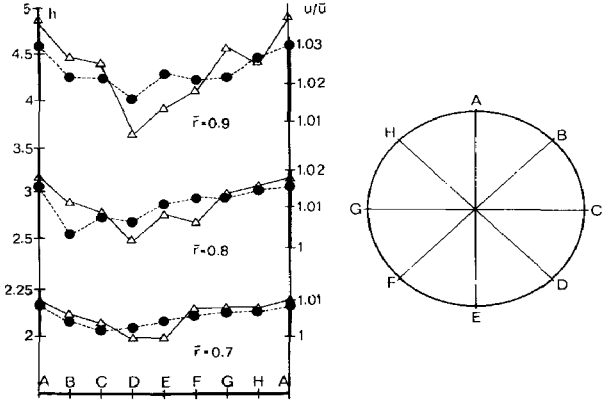

Fig. 7. Variation of h (△) and $u/\bar{u}$ (●) for several radial positions with the angular direction for the stainless-steel column.

although this pattern gradually vanishes for smaller $\bar{r}$ values. At any given radial distance, the relative standard deviation of h over the A–B–C . . . G–A range can be taken as an index of radial symmetry. The results are shown in Fig. 8. The larger scatter for the classical column is a further indication of a highly disturbed wall region compared with the Teflon column, which exhibits a more regular packing structure.

It is likely that the quasi-perfect symmetry of the newly introduced columns is responsible for their good reproducibility from packing to packing. Conversely, the wall effect appears to be the main cause of the poorer reproducibility of classical columns. More data are needed before any definite conclusion can be drawn.

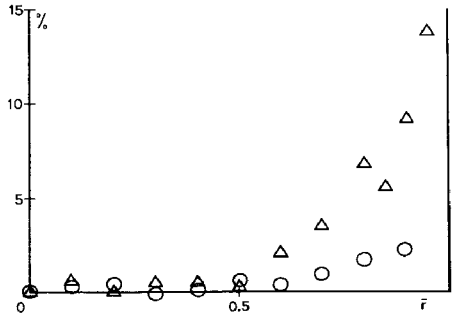

Fig. 8. Angular symmetry index for the classical column (△) *versus* the radially compressed column (○).

At this stage it may be appropriate to suggest a potential benefit of obtaining more homogeneously packed large-diameter columns of the Teflon type. In addition to better performances, these columns might be used for differential refractive index detection under gradient concentration operating conditions.

By analogy with the dual polarographic detector, the two refractive index detector circuits can be fed from two separate pick-up tubes, the location of which is such that (1) the corresponding plate heights are similar, and (2) one pick-up is virtually free from solute while the other is coincident with the injection source. The diameter of the pick-up zones should be as large as is allowed by the column heterogeneity. Preliminary experiments have led to a 150-fold reduction in the baseline drift; further experiments aimed at optimizing this system are being carried out. The results will be published separately[26].

Axial and radial dispersion in relation to the overall band second moment

All of the preliminary findings advocate in favour of radially compressed columns. However, the extent of the potential gain is unclear for the analyst whose only concern is the overall axial diffusivity. It is therefore essential to have some indication of how h_a, h_r and $u/\bar{u}$ contribute to the overall column plate height. This raises the problem of knowing the conventional plate heights for the two columns as the solute becomes increasingly exposed to the wall. Experimentally, it was only necessary to use a classical conical-shaped terminator to interface the detector to the column. A single "working" platinum electrode was used to monitor the concentration of the solute from the terminator exit. The reverse-flow technique was used in order to increase the radial dispersion by artificially increasing the equivalent length of the column. The results are reported in Fig. 9. Again $\nu = 100$ was chosen for internal consistency and experimental convenience. It can be seen that h gradually increases with increasing equivalent column length, *i.e.*, the solute concentration in the wall-disturbed region (see Fig. 4). Eventually h reaches a plateau: the loss is significant and is much more pronounced for the classical column than for the Teflon column.

It should be noted that, because the wall extends over 25–30 particle diameters, the first Knox and Parcher criterion (eqn. 10 from ref. 15) for virtually no wall effect is inadequate. Transposed to our nomenclature, this would make the "transition" occur at $L/L_1 = 4$. Fig. 9 disqualifies this rule. This situation was recognized by Knox *et al.*[16],

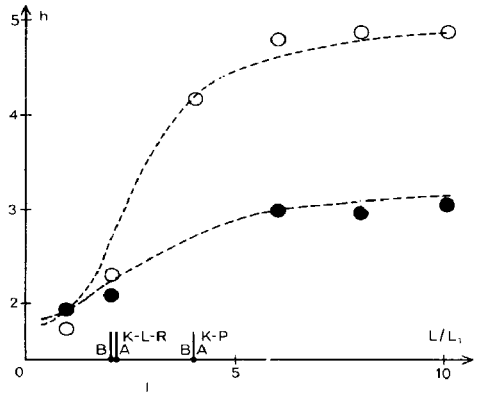

Fig. 9. Column reduced plate height for $\nu = 100$ as a function of the column (equivalent) length. (A) Classical column; (B) radially compressed column. Broken lines, best fit obtained from eqn. 12. K–P represents the Knox and Parcher criterion and K–L–R represents the Knox, Laird and Raven criterion (see text).

who proposed a modified criterion which appears to be much more realistic and well adapted for practical column design. Fig. 9 shows that it successfully predicts the "transition" range, although it should be realized that no column is ever completely free from any wall effect.

The results in Fig. 9 also illustrate the difficulties encountered when comparing column performances. For example, it is difficult to decide which of the two columns is better. Column B is better than column A with long columns whereas the two columns exhibit equally good properties for short columns. Also it is difficult to know how many published data and comparisons are erroneous or misleading as a result of the wall effect. It should be pointed out that the behaviour shown in Fig. 9 can hardly be extrapolated to other velocities or columns. For example, the dry packing procedure used here may not lead to optimal packing in the vicinity of the wall compared with that obtained by the slurry technique, in that the particle size segregation may be more significant[5].

Nevertheless, we believe that the gradual increase in h and the attainment of a plateau is a general pattern for all columns and only the extent of the loss of efficiency is expected to vary from system to system.

As expected, the relationship between results in Figs. 4, 5 and 6 and the overall plate height is complex, mainly because of the ill-defined nature of the $(u/\bar{u})_r$ ratio. All of the results in Fig. 9 can be accounted for on the basis of a semi-theoretical model. From the definition of the centred second moment m_2, it is obvious that, at any fixed time after the injection

$$m_2 = 2 \int_0^1 \bar{r} \int_{-\infty}^{+\infty} (l - \bar{u}t)^2 \, C(l, \bar{r}, t) \quad \mathrm{d}(l - \bar{u}t) \, \mathrm{d}\bar{r} \tag{8}$$

where l is the longitudinal position with respect to the injection point. Eqn. 8 assumes a doubly infinite column length for mathematical convenience and, of course, it should be normalized accordingly. For a given radial position, the peak maximum may not

coincide with the centre of gravity of the peak. Let us define its position, $l_{(\bar{r})}^{\max}$, through a factor $\alpha(\bar{r})$ such that

$$l_{(\bar{r})}^{\max} = \bar{u}t\,[1 + \alpha(\bar{r})] \tag{9}$$

Assuming that the axial solute normalized concentration profile, $C(\bar{r})$ at any given radial position can be expressed as a gaussian function, then, by virtue of eqn. 9, we obtain

$$C(\bar{r}) = \frac{1}{\sigma_a(\bar{r})\sqrt{2\pi}} \cdot \exp\left\{-\tfrac{1}{2}\left[\frac{\bar{u}t - l + \alpha\bar{u}t}{\sigma_a(\bar{r})}\right]^2\right\} \tag{10}$$

The axial variance at any radial distance is obtained from $h_a(\bar{r})$ (Figs. 5 and 6) through

$$\sigma_a(\bar{r}) = [h_a(\bar{r})\,\bar{u}t\mathrm{d}p]^{1/2} \tag{11}$$

By combining eqns. 8, 9 and 10, the band overall second moment becomes

$$m_2 = \frac{\displaystyle\int_0^1 \bar{r}\,C_{(\bar{r})}^{\max}\sigma_a(\bar{r}) \int_{-\infty}^{+\infty} \frac{(l-\bar{u}t)^2}{\sigma_a(\bar{r})\sqrt{2\pi}} \cdot \exp\left\{-\tfrac{1}{2}\left[\frac{\bar{u}t - l + \alpha(\bar{r})\bar{u}t}{\sigma_a(\bar{r})}\right]^2\right\} \cdot \mathrm{d}(l-\bar{u}t)\,\mathrm{d}\bar{r}}{\displaystyle\int_0^1 \bar{r}C_{(\bar{r})}^{\max}\,\sigma_a(\bar{r})\,\mathrm{d}\bar{r}} \tag{12}$$

where the denominator is the normalizing factor. $C_{(\bar{r})}^{\max}$ is calculated from eqn. 6. It should be noted that the middle integral

$$\int_{-\infty}^{+\infty} \cdots\, \mathrm{d}(l-\bar{u}t) = \sigma'^2_{a(\bar{r})} \tag{13}$$

has the dimension of a pseudo variance $\sigma'^2_{a(\bar{r})}$; it equals $\sigma^2_{a(\bar{r})}$ when $\alpha = 0$. Because of the definition of reduced plate height, it is convenient to take $\sqrt{L}\mathrm{d}p$ as the unit of length for expressing l, $\bar{u}t$ and σ; this turns m_2 into h. Evaluation of the $\alpha(r)$ term can be carried out as follows. When the $u/\bar{u}$ function, for a given column length, is known, as in Figs. 5 and 6, eqn. 9 implies that

$$\alpha(\bar{r}) = (u/\bar{u})_{\bar{r}} - 1 \tag{14}$$

Now let us assume that the column is lengthened at constant velocity, and consider what the new α would be. The only safe means of obtaining the correct answer would be to carry out the experiment, but as we are dealing with a semi-empirical model a certain degree of approximation can be tolerated. The variation of radial velocity with radius causes the pulse to spread axially; however, radial diffusion counteracts this by causing the tracer that has been carried ahead in the faster flow to diffuse radially into the slower flow, and likewise the tracer that has been held back in the slower flow diffuses into the faster flow. This results in a sharper zone that would be obtained if α was constant. Hence α is dependent on length.

It seems reasonable to assume that α varies in such a way that $\sigma'^2_{a(\bar{r})}$, from eqn. 13, is proportional to the column length, as only this assumption leads to a constant value of h at large enough L. Hence it is only necessary to know $\alpha(\bar{r})$ at a certain given

length in order to be able to solve eqn. 12. A final difficulty arises in evaluating $\sigma_a(\bar{r})$, that is $h_a(\bar{r})$, over the range 0–1. It was found impossible to obtain meaningful measurements at a closer distance to the wall than those reported in Figs. 5 and 6. The lack of values in the most disturbed region of the packing is infortunate for two reasons: firstly, $h(\bar{r})$ increases sharply in the vicinity of the wall, and secondly, the integration over the column cross-section turns $\bar{r}$ into a weighting factor (see eqn. 12). Hence, the properties of the very first layers may significantly affect the overall second moment m_2. Because any extrapolation would be hazardous, it was chosen to regard the reduced plate height at the bed–wall interface, $h(1)$, as an adjustable parameter, the value of which could be calculated from a least-squares fitting of Fig. 9 with the help of eqn. 12. The integration were carried out using Simpson's rule. The goodness of the fit, which can be appreciated from Fig. 9, validates the practical use of eqn. 12. The adjusted $h(1)$ values are 14.8 ± 1.5 units for the classical column and 3.8 ± 0.4 units for the radially compressed column. Unless the model is physically meaningless, it can be concluded that the use of a radially compressed flexible wall considerably improves the packing order of the region adjacent to the wall, presumably because the wall adjusts its form to that of the bed.

The exceedingly large h values at the wall interface of the classical column probably indicates that a high degree of bridging occurs as a result of the presence of the wall.

CONCLUSIONS

It has been shown that, with central injection, the plate height varies with the column length. The efficiency is optimal for very short columns and gradually deteriorates as the column length increases. Eventually the plate height reaches a plateau, which indicates that the wall effect is at a maximum. The loss of efficiency experienced in this study is significant, although hopefully it will be smaller for the best analytical columns available today as it should depend on the packing procedure. Nevertheless, the dependence of the efficiency on the column length raises serious doubts about the meaningfulness of some published plate height coefficients.

On a more practical basis, this study also revealed that the use of radially compressed columns appreciably attenuates the wall-induced deterioration of efficiency. The improvement, which is significant, justifies further studies on the capabilities of radially compressed soft-walled columns.

ACKNOWLEDGEMENTS

I am grateful to D. Vachon for technical assistance. I also acknowledge the Canadian Research Council for partial support of this work under grant A 0523.

REFERENCES

1 F. H. Huyten, W. van Beersum and G. W. A. Rijnders, in R. P. W. Scott (Editor), *Gas Chromatography 1960*, Butterworths, London, 1960, p. 224.
2 S. T. Sie and G. W. A. Rijnders, *Anal. Chim. Acta*, 38 (1967) 3.
3 G. J. Frisone, *J. Chromatogr.*, 6 (1961) 97.
4 J. C. Giddings, *J. Gas Chromatogr.*, 1 (1963) 12.

5 J. C. Giddings and E. N. Fuller, *J. Chromatogr.*, 7 (1962) 255.
6 A. B. Littlewood, in A. Goldup (Editor), *Gas Chromatography 1964*, Institute of Petroleum, London, 1964, p. 77.
7 A. B. Littlewood, *Anal. Chem.*, 38 (1966) 2.
8 K. P. Hupe, U. Busch and K. Winde, *J. Chromatogr. Sci.*, 7 (1969) 1.
9 M. J. E. Golay, in H. J. Noebels, R. F. Wall and N. Brenner (Editors), *Gas Chromatography, Second International Symposium, 1959*, Academic Press, New York, 1961, Ch. 2.
10 J. C. Sternberg and R. E. Poulson, *Anal. Chem.*, 36 (1964) 58.
11 C. E. Schwartz and J. M. Smith, *Ind. Eng. Chem.*, 45 (1953) 1209.
12 J. R. Conder, in H. Purnell (Editor), *New Developments in Gas Chromatography*, Wiley, New York, 1973, p. 137.
13 J. H. Knox, *Anal. Chem.*, 38 (1966) 257.
14 D. S. Horne, J. H. Knox and L. McLaren, *Separ. Sci.*, 1 (1966) 531.
15 J. H. Knox and J. F. Parcher, *Anal. Chem.*, 41 (1969) 1599.
16 J. H. Knox, G. R. Laird and P. A. Raven, *J. Chromatogr.*, 122 (1976) 129.
17 J. C. Giddings, *Dynamics of Chromatography, Part 1*, Marcel Dekker, New York, 1965.
18 J. J. de Stefano and H. C. Beachell, *J. Chromatogr. Sci.*, 10 (1972) 654.
19 J. J. de Stefano, in L. L. Snyder and J. J. Kirkland, *Introduction to Modern Liquid Chromatography*, Wiley, New York, 1974, Ch. 12.
20 J. N. Little, R. L. Cotter, J. A. Prendergast and P. D. McDonald, *J. Chromatogr.*, 126 (1976) 439.
21 L. L. Snyder and J. J. Kirkland, *Introduction to Modern Liquid Chromatography*, Wiley, New York, 1976.
22 J. H. Knox, J. Durand and G. R. Laird, *Proc. Soc. Anal. Chem.*, 11 (1974) 310.
23 P. G. Saffman, *J. Fluid Mech.*, 6 (1959) 321.
24 P. G. Saffman, *J. Fluid Mech.*, 7 (1960) 194.
25 A. Klinkenberg, H. J. Krajenbrink and H. A. Lauwerier, *Ind. Eng. Chem.*, 45 (1953) 1202.
26 C. Eon, to be published.